The Astrophysical Journal, 668:906–917, 2007 October 20

MASSIVE CLUMPS IN THE NGC 6334 STAR-FORMING REGION

Diego J. Muñoz, Diego Mardones, Guido Garay, and David Rebolledo
Departamento de Astronomía, Universidad de Chile, Santiago, Chile; dmunoz@cfa.harvard.edu

Kate Brooks
Australia Telescope National Facility, Epping NSW 1710, Australia

and

Sylvain Bontemps
Observatoire de Bordeaux, 33270 Floirac, France
Received 2007 January 11; accepted 2007 June 19

ABSTRACT

We report observations of dust continuum emission at 1.2 mm toward the star-forming region NGC 6334 made with the SEST SIMBA bolometer array. The observations cover an area of $\sim$2 deg^2 with approximately uniform noise. We detected 181 clumps spanning almost 3 orders of magnitude in mass ($3–6 \times 10^3\ M_\odot$) and with sizes in the range 0.1–1.0 pc. We find that the clump mass function $dN/d\log M$ is well fit with a power law of the mass with exponent -0.6 (or equivalently $dN/dM \propto M^{-1.6}$). The derived exponent is similar to those obtained from molecular line-emission surveys and is significantly different from that of the stellar initial mass function. We investigated changes in the mass spectrum by changing the assumptions on the temperature distribution of the clumps and on the contribution of free-free emission to the 1.2 mm emission and found little change on the exponent. The cumulative mass distribution function is also analyzed, giving consistent results in a mass range excluding the high-mass end, where a power-law fit is no longer valid. The masses and sizes of the clumps observed in NGC 6334 indicate that they are not direct progenitors of stars and that the process of fragmentation determines the distribution of masses later on or occurs at smaller spatial scales. The spatial distribution of the clumps in NGC 6334 reveals clustering which is strikingly similar to that exhibited by young stars in other star-forming regions. A power-law fit to the surface density of companions gives $\Sigma \propto \theta^{-0.62}$.

Subject headings: stars: formation

On-line material: machine-readable table

1. INTRODUCTION

1.1. *Massive Star Formation and Molecular Cloud Structure*

Half of the mass in the interstellar medium is in the form of molecular gas exhibiting a broad range of structures, ranging from small isolated clouds of a few solar masses and subparsec sizes to giant molecular clouds (GMCs), with masses of several times $10^6\ M_\odot$ and sizes of 100 pc (Blitz 1993). We adopt the nomenclature used in the review of Williams et al. (2000) to refer to the different observed molecular structures. GMCs are the sites of most of the star formation activity in the Milky Way, in particular of high-mass stars, which are usually born in clusters within massive cores. In order to understand how massive cores form from the GMC complexes, we must understand how fragmentation and condensation proceed within them. It is essential for this purpose to determine the physical properties of complete samples of massive cores within GMCs.

Molecular line surveys, at millimeter and submillimeter wavelengths, have revealed the structure of GMCs to be highly inhomogeneous and clumpy (Blitz 1993; Evans 1999). These surveys have shown that the mass spectra of clouds (Sanders et al. 1985; Solomon et al. 1987), clumps (Blitz 1993; Kramer et al. 1998; Lada 1999; Williams et al. 2000), and total mass of embedded clusters (Lada & Lada 2003) are similar to one another. These mass spectra are notably different than the stellar mass spectrum: the initial mass function (IMF; Salpeter 1955). In particular, several works on molecular line mapping of GMCs show that their mass spectra follow a power law with nearly the same exponent, $x \sim 0.6$, where $dN/d\log M \propto M^{-x}$ (e.g., Blitz 1993; Williams et al. 2000).

The development of large bolometer arrays during the last 10 years has made it possible to carry out extended millimeter and submillimeter continuum surveys, allowing the direct dust mass determination of clumps. Motte et al. (1998) mapped the Ophiuchus cloud with the IRAM 30 m telescope and found a distribution of clump masses similar to Salpeter's IMF. Several works (Johnstone et al. 2001; Beuther & Schilke 2004; Mookerjea et al. 2004; Reid & Wilson 2005; Johnstone et al. 2006) have reported mass spectra of dust cores with indexes similar to Salpeter's IMF and different from those derived from molecular line studies. If the mass function of cores is similar to the Salpeter IMF, independent of the range of masses involved, then the star formation process within GMCs would be defined in the earliest stages as a result of cloud fragmentation.

In this paper we present a large-scale 1.2 mm continuum study of the NGC 6334 GMC aimed to find and study a complete sample of massive cores.

1.2. *NGC 6334 and NGC 6357*

NGC 6334 is one of the nearest and most prominent sites of massive star formation, at a distance of only 1.7 kpc (Neckel 1978). The central region of NGC 6334 consists of a $\sim$10 pc long filament with seven sites of massive star formation. Within them there is a wide variety of activity associated with star formation,

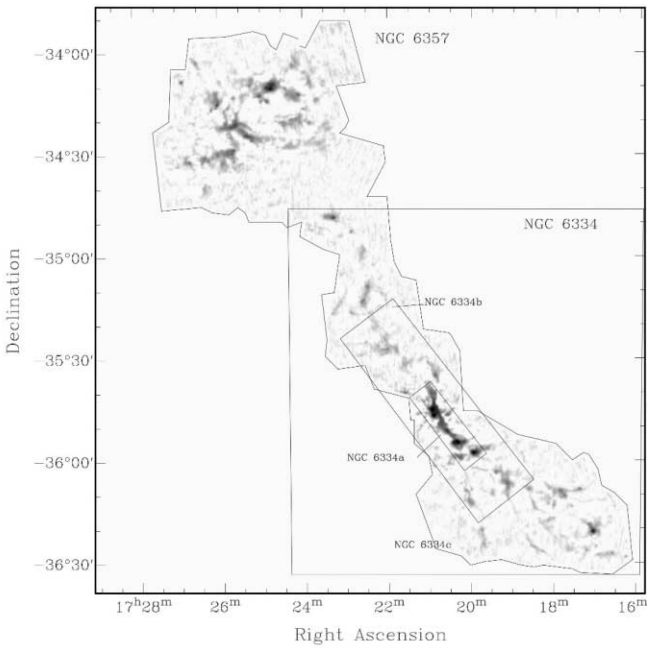

FIG. 1.—Gray-scale image of the 1.2 mm emission toward NGC 6334 and NGC 6357. The polygonal line was used to exclude the noisy borders of the mapped region. The large square indicates the area defined as NGC 6334 in the present analysis. It encloses 182 of the 347 clumps found using `clfind2d`. Also labeled are the three subregions chosen for statistical analysis: the central region NGC 6334a (see Fig. 2); a larger extension NGC 6334b; and finally NGC 6334c, which includes only the clumps outside of NGC 6334b. [*See the electronic edition of the Journal for a color version of this figure.*]

such as water masers, H II regions (Rodríguez et al. 1982; Carral et al. 2002), and molecular outflows.

Early far-infrared (FIR; McBreen et al. 1979) and radio (Rodríguez et al. 1982) surveys characterized the overall properties of the main sites of massive star formation, whereas near-infrared (NIR) studies (Straw et al. 1989; Straw & Hyland 1989) revealed the cluster-forming nature of many of these sites. Kraemer & Jackson (1999) and Burton et al. (2000) review the different notations used by previous authors to identify bright sources. Submillimetric and millimetric results on NGC 6334 have been previously reported by Gezari (1982), Sandell (2000), and McCutcheon et al. (2000), all of whom focused in the northern portion of the main filament: sources I and I(N), which have been recently resolved into smaller cores (Hunter et al. 2006). In the case of Sandell (2000) sources I and I(N) were redefined as the central peaks of each respective source. This showed, following observations at 350 μm, 450 μm, 380 μm, 1.1 mm, and 1.3 mm showed inner structure for Gezari's cores. In Sandell (2000) sources, I and I(N) have angular sizes of $10'' \times 8''$ and $11'' \times 8''$, respectively. These sizes are $\sim$10 times smaller than our massive clumps cl1 and cl2, identified as I and I(N), respectively. For the present work cl1 encloses sources I and I(NW) of Sandell's nomenclature, while cl2 encloses I(N), SM1, SM2, SM4, and SM5, as well as considerable extended emission in both cases. Hence, comparison between that work and ours is not straightforward.

Following the evolutionary sequence proposed by Beuther et al. (2006), NGC 6334 and NGC 6357 appear to be in an intermediate phase of massive starless clumps and protoclusters. The latter region seems more evolved than the former, since compact H II regions are still prominent in NGC 6334 at radio wavelengths, while the structure of NGC 6357 is more disrupted, suggesting that massive stars have already shaped the mother clouds. This finding is also supported by the presence of more infrared sources in NGC 6357. From this evidence, as well as the lack of significant amounts of cold material in between the two regions, we consider NGC 6334 and NGC 6357 as two independent regions, defining NGC 6334 as the southeastern portion of the map shown in Figure 1.

Even though NGC 6334 is one of the closest GMCs, it is still far compared to low-mass star-forming regions (e.g., Ophiuchus, Orion B, and Taurus). As a consequence, the detected clumps in NGC 6334 are larger and considerably more massive, and can be considered likely cluster-forming cores (Motte et al. 2003; Ward-Thompson et al. 2006; Beuther et al. 2006), and we are unable to resolve their inner structure.

2. OBSERVATIONS AND DATA REDUCTION

The regions NGC 6334 and NGC 6357 were mapped using the 37-channel SEST Imaging Bolometer Array (SIMBA) in the fast-mapping mode in three different epochs: 2002 July, September, and 2003 May. The passband of the bolometer has an equivalent width of 90 GHz and is centered at 250 GHz (1.2 mm). The half-power beamwidth of the instrument is $24''$, giving a spatial resolution of 0.2 pc. Ninety-five observing blocks were taken toward the NGC 6334 and NGC 6357 regions, with typical extension of $\sim 10' \times 20'$, to sample a total area of $\sim$2 deg^2 between $17^{\rm h}16^{\rm m}00^{\rm s}$, $-36^\circ 40' 00''$ and $17^{\rm h}28^{\rm m}00^{\rm s}$, $-33^\circ 40' 00''$. Sky-dip observations were done approximately every 2 hr to determine the zenith opacity at 250 GHz. Typical opacities were $\tau \approx 0.2$, with values ranging from 0.17 to 0.4 in a few cases. We also checked pointing on η Carinae every 2 hr and found a typical rms deviation of $3''$–$5''$ in azimuth and elevation. Every night we observed Uranus for flux calibration.

The SIMBA data were reduced using the MOPSI program, written by Robert Zylka, after conversion by the `simbaread` program, written at ESO. The SIMBA raw data consists of a time series for each of the 37 bolometers (channels) in the array. The time series includes the counts per channel and sky position. The reduction procedure first removes the brightest data spikes. Next a low-order baseline in time is fit to the full observation file for each channel, and a zero-order baseline is fit in azimuth for each channel. The data are then deconvolved by the time response function of each channel, as measured by the SEST staff. Gain elevation and extinction corrections are applied next. An iterative sky noise reduction procedure is then applied, where the counts of each channel are correlated with those of the other 36 channels, yielding a so-called flat-field correction to calibrate the relative sensitivity of each pixel. A source image is finally produced by averaging the flux of all channels as they pass through the same position on the sky.

The sky-noise reduction algorithm includes the flux coming from both the source and the sky simultaneously. If the source extends over several channels, this introduces spurious correlated flux, which hampers the sky-noise reduction procedure. To avoid this problem, a smoothed model of the source flux distribution on the sky is subtracted from the raw time series data. Thus, the sky-noise reduction procedure can be repeated, finding a better source model with each iteration.

The calibration was derived from maps of Uranus. The resulting multiplicative factor varied between 0.06 and 0.09 Jy count^{-1} beam^{-1}. Finally, reduced images were combined using the MOPSI software to produce the final map (Fig. 1). In order to reduce noise further, a Gaussian smoothing of $30''$ was applied to the final image

TABLE 1
Radio, FIR, and Millimeter Sources in NGC 6334

Radio Name	Radio Position		FIR Name	FIR Position		SIMBA Name	SIMBA Position		References
	α (J2000.0)	δ (J2000.0)		α (J2000.0)	δ (J2000.0)		α (J2000.0)	δ (J2000.0)	
G351.20+0.70	17 20 04.1−35 56 10	δ (J2000.0)				cl210	17 19 58.0	−35 55 56	4, †
Unnamed[a]			V	17 19 57.4	−35 55 56	cl4	17 19 56.7	−35 55 56	2, †
A	17 20 19.2	−35 55 56	IV	17 20 20.7	−35 55 56	cl3 (cl7, cl15)	17 20 19.8	−35 55 56	1, 2, †
C	17 20 32.6	−35 55 56	III	17 20 31.3	−35 55 56	cl11	17 20 34.2	−35 55 56	1, 2, †
D	17 20 44.3	−35 55 56	II	17 20 42.2	−35 55 56	cl19	17 20 42.8	−35 55 56	1, 2, †
E	17 20 50.9	−35 55 56	...	...		...	...		1
F	17 20 53.4	−35 55 56	I	17 20 55.1	−35 55 56	cl1	17 20 54.0	−35 55 56	1, 2, †
			I(N)	17 20 53.6	−35 55 56	cl2	17 20 56.0	−35 55 56	3, †

Notes.—Units of right ascension are hours, minutes, and seconds, and units of declination are degrees, arcminutes, and arcseconds. The FIR and radio equatorial coordinates have been precessed from B1950.0 to J2000.0.

[a] The radio counterpart for FIR source V is observed at 1.6 GHz with similar peak intensity to G351.20+0.70, but was not identified earlier as an H II region but as part of a PDR shell (Moran et al. 1990; Jackson & Kraemer 1999; Burton et al. 2000).

References.—(1) Rodríguez et al. 1982; (2) McBreen et al. 1979; (3) Gezari 1982; (4) Moran et al. 1990; † this work.

and the map edges were removed. The typical rms noise of the final map is 25 mJy beam^{-1}. SIMBA observations usually have an absolute flux uncertainty of ∼20% (Faúndez et al. 2004).

3. RESULTS

3.1. *Clump-finding Algorithms*

Different clump-finding algorithms have been used to study the substructure in molecular clouds. Among the most used are `clumpfind` (Williams, de Geus & Blitz 1994) and `gaussclumps` (Stutzki & Güsten 1990). The two algorithms have different biases but find similar clump distributions (e.g., Schneider & Brooks 2004). We use the `clumpfind` algorithm because it makes no assumptions about inherent clump shapes. `Clumpfind` first finds the brightest emission peak in the image, then it descends to a lower contour level and finds all the image pixels above this level, associating them to the first peak (clump) if contiguous, or else it defines one or more additional clumps. The spatial separation of clumps is defined along saddle points. We used a conservative lower detection threshold of 75 mJy (3 σ) per beam. We found 347 clumps in the whole image, 182 of which are in the NGC 6334 region. Only two clumps are likely to be fictitious, judging from their small effective radii and location close to the borders, and only one of them is in the NGC6334 region. Thus, we use the remaining 181 clumps in our analysis of the region NGC 6334 in this paper. Table 1 lists the clumps in our sample associated with previously known radio and IR sources. These sources are all located in the brightest part of the filament as seen in Figure 2.

3.2. *Clump Size Distribution*

Figure 3 shows a histogram of the clump size distribution. The effective radius, or size, is determined from the angular area encompassed by each clump (from the `clfind2d` output), assuming a distance to NGC 6334 of 1.7 kpc. The sizes range from 0.1 to 1.0 pc, with a median of 0.36 pc. These values are similar to those derived for clumps within GMCs (Blitz 1993; Williams

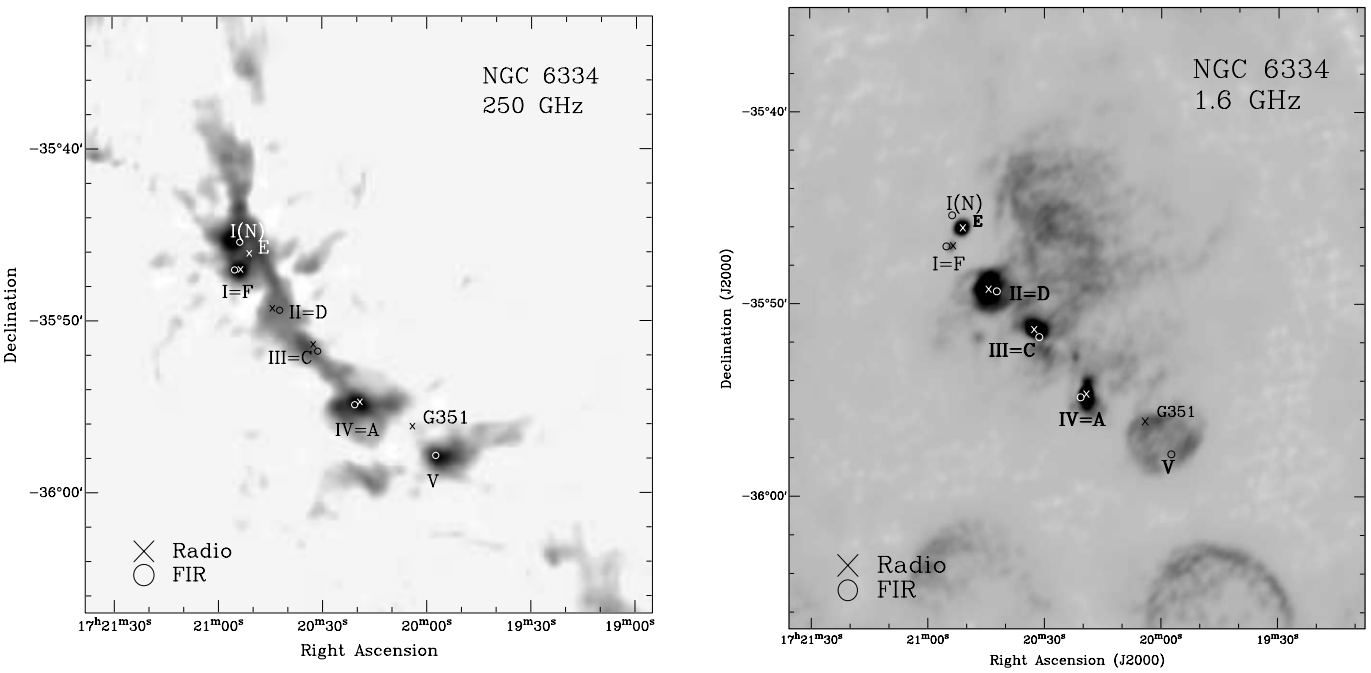

Fig. 2.—Peak position of the radio and FIR sources of Table 1 plotted over images of the SIMBA continuum at 250 GHz (*left*) and ATCA continuum at 1.6 GHz (*right*). [*See the electronic edition of the Journal for a color version of this figure.*]

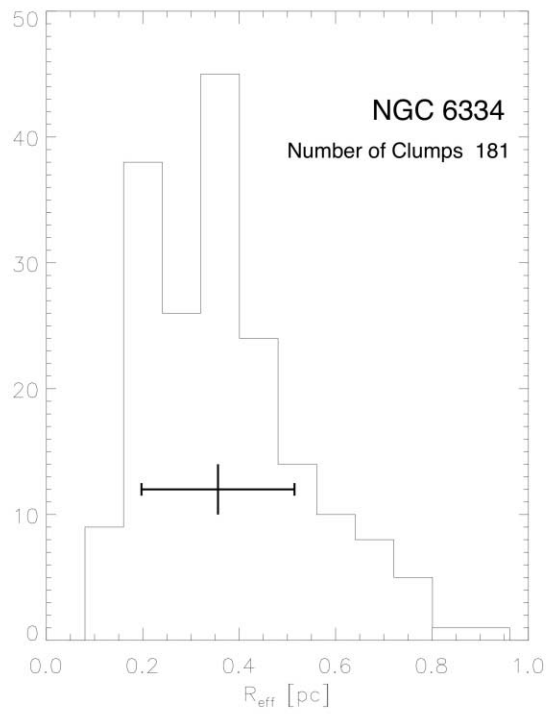

FIG. 3.—Clump size distribution (in pc) assuming a distance of 1.7 kpc to NGC 6334. The cross below the histogram indicates the median and standard deviation of the distribution.

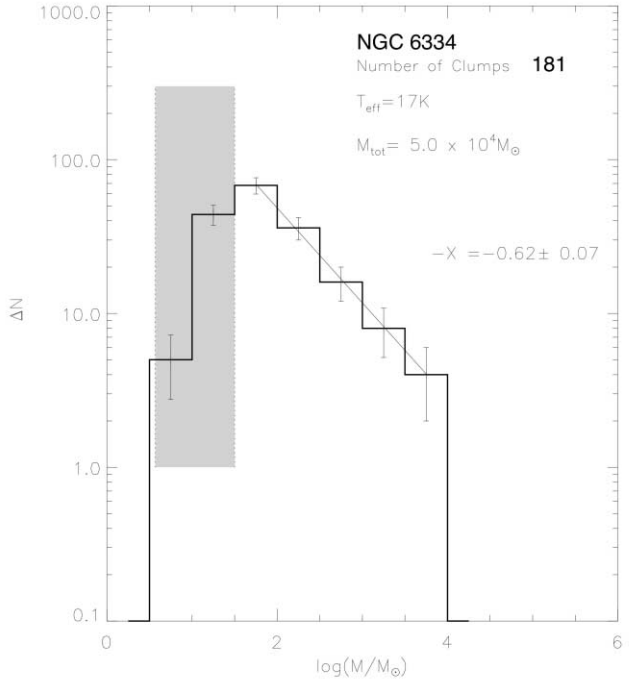

FIG. 4.—Mass histogram of the clumps within NGC 6334. ΔN is the number of clumps in bins of constant $\Delta \log M$ (=0.5). The shaded region delimits the 3 σ detection limit and our estimated completeness limit. This region is excluded from the least-squares fit.

et al. 2000; Pudritz 2002; Faúndez et al. 2004; Beuther et al. 2006).

3.3. *Mass Estimates*

Since the dust emission at 1.2 mm is most likely to be optically thin (e.g., Garay et al. 2002), the mass of each clump can be estimated from the observed flux density. For an isothermal dust source, the total gas mass M_g is related to the observed flux density S_ν at an optically thin frequency ν as (see Chini et al. 1987)

$$M_g = \frac{S_\nu D^2}{R_{\rm dg}\kappa_\nu B_\nu(T_d)}, \tag{1}$$

where κ_ν is the dust mass absorption coefficient, D is the source distance, $R_{\rm dg}$ is the dust-to-gas mass ratio, and B_ν is the Planck function. In more convenient units the gas mass can be written as

$$M_g = 20.4\left(\frac{S_{250\rm GHz}}{\rm Jy}\right)\left(\frac{D}{\rm kpc}\right)^2\left(\frac{0.01}{R_{\rm dg}}\right) \times \left(\frac{1\ {\rm cm^2\ g^{-1}}}{\kappa_{250\rm GHz}}\right)\left(e^{12{\rm K}/T_d}-1\right) M_\odot. \tag{2}$$

Using a dust-mass absorption coefficient of $\kappa_{250\rm GHz} = 1\ {\rm cm^2\ g^{-1}}$ (Ossenkopf & Henning 1994); a dust-to-gas ratio of 0.01; a distance of 1.7 kpc, and a dust temperature $T_d = 17$ K,[1] we computed the mass of each clump found by `clfind2d`. We find that the clump masses in NGC 6334 range from 3 to 6000 $M_\odot$, with a mean value of 170 $M_\odot$ and a median value of 60 $M_\odot$. The total mass of the clumps in NGC 6334 is $M_{\rm tot} \sim 5 \times 10^4\ M_\odot$.

3.4. *Clump Mass Spectrum*

The clump mass function (CMF), $\xi_\alpha(M)$, is defined as the number of clumps per unit mass,

$$\xi_\alpha(M) = \frac{dN}{dM} \approx \frac{\Delta N}{\Delta M}, \tag{3}$$

where ΔN and ΔM are used to indicate observational estimates. Some workers prefer to use a *logarithmic* CMF, ξ_x, defined as the number of clumps per unit logarithmic mass:

$$\xi_x(M) = \frac{dN}{d(\log M)} \approx \frac{\Delta N}{\Delta(\log M)}. \tag{4}$$

These two functions are related by the expression $\xi_x(M) = (M \ln 10)\xi_\alpha(M)$. If $\xi_\alpha(M)$ has a power-law dependence with mass, $\xi_\alpha(M) \propto M^{-\alpha}$, then the logarithmic CMF should also have a power-law dependence with mass, $\xi_x(M) \propto M^{-x}$, where the power-law exponents are related by $x = \alpha - 1$. A Salpeter slope corresponds to $x = 1.35$, or $\alpha = 2.35$.

The CMF is usually estimated from a histogram of the derived clump masses, assuming it has a power-law form. The distinction between the observationally derived ξ_α and ξ_x is made by Scalo (1998), Kroupa (2001), and Larson (2003). Its implications in the type of binning used in the histogram are also mentioned in Klessen & Burkert (2000). Figure 4 shows a histogram of the mass of the clumps within NGC 6334. The bin size $\Delta \log M$

[1] We choose a value of 17 K because it lies in the typical range for cold dark clouds (Pudritz 2002). It is also a factor of 2 smaller 34 K—the average temperature of clouds with infrared counterparts (Faúndez et al. 2004)—making the comparison between both temperatures easier.

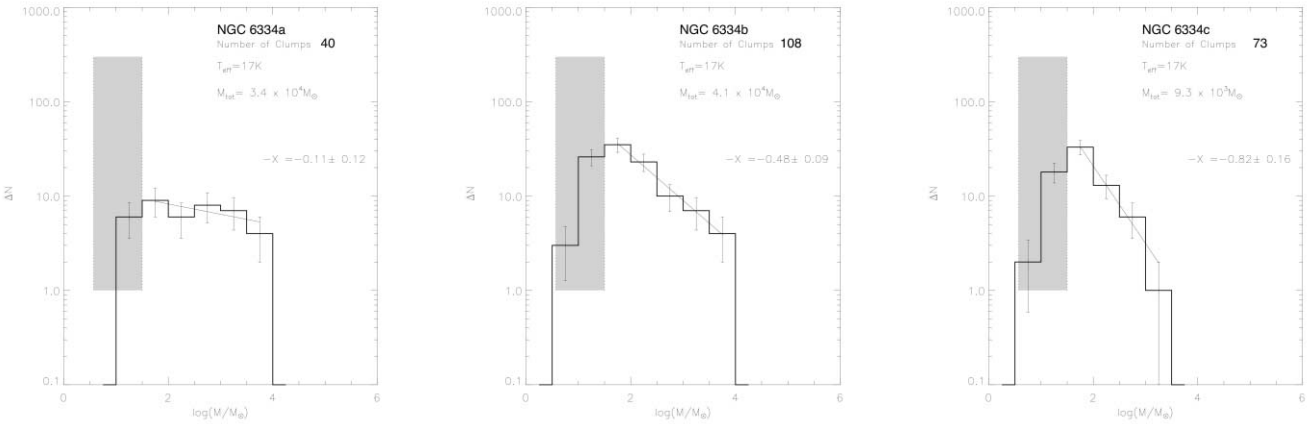

FIG. 5.—Mass histogram of clumps within selected regions of NGC 6334 (see Fig. 1). *Left*: NGC 6334a, $x = 0.11$. *Center*: NGC 6334b, $x = 0.48$. *Right*: NGC 6334c, $x = 0.82$.

has a constant value of 0.5. The completeness limit is estimated to be $\sim 30\ M_\odot$. A least-squares linear fit to the ΔN versus $\log M$ relationship gives a slope of -0.62 ± 0.07.

Variations of the CMF within NGC 6334.—Given the large number of clumps in our survey, we can assess possible changes in the CMF as a function of position within the cloud. We consider the three subregions within NGC 6334 defined in Figure 1 and construct a mass spectrum for each of them (see Fig. 5). The CMF in NGC 6334a, which encompasses the central filament containing the most massive clumps and where star formation is clearly taking place, is well fitted with a power law with an exponent of $x = 0.11 \pm 0.12$, significantly shallower than the value determined for the whole sample. The exponent steepens for NGC 6334b ($x = 0.48$), which covers a much larger region than the central filament. For NGC 6334c, which excludes the main filament, the slope is even steeper, $x = 0.82$. Thus, the slope of the CMF in NGC 6334 depends on the location of the clumps within the cloud.

Out of the total mass of $5 \times 10^4\ M_\odot$ in 181 dense massive clumps in NGC 6334, $3.4 \times 10^4\ M_\odot$ are contained within the NGC 6334a region and $1.6 \times 10^4\ M_\odot$ are outside. The slope of the CMF of the whole region is dominated by the relatively low-mass clumps in the outer region, since they dominate by number. The bulk of the cloud mass is located in a few inner clumps, which do not affect significantly the exponent of the derived CMF. This could shed light on the effects of the star formation activity, mass segregation, or coalescence in the clump mass spectrum within GMCs. We know that it is more likely to miss low-mass clumps due to confusion within the region NGC 6334a than in the outer regions under study. This bias naturally flattens the slope of the mass spectrum in the inner region. However, we find in § 3.6.1 that clumps are not only concentrated by mass toward the center, but also by number, hinting that this result is partly real. Higher angular resolution observations will be needed to settle this issue.

3.5. *Possible Uncertainties in the CMF*

In the above analysis we assumed a single temperature for the whole ensemble of clumps. This is clearly an approximation; the clumps themselves are not isothermal, and the temperature is likely to be different from clump to clump. In addition, we assumed that all the detected 1.2 mm emission is due to dust thermal emission. It is possible, however, that some of the 1.2 mm emission is due to free-free emission from ionized gas. In what follows we assess these two assumptions and quantify their effects on the derived CMF.

3.5.1. *Temperature*

Assuming that all clumps within a GMC are isothermal and have the same temperature is clearly a rough approximation. In particular, clumps with already formed stars are expected to be warmer than clumps with no signs of embedded objects. Beuther & Schilke (2004) have argued that this assumption introduces an uncertainty in the derived slope of the mass spectrum. If higher temperatures are adopted for the more massive clumps, their derived masses will decrease, whereas if lower temperatures are adopted for the less massive clumps, their derived masses will increase: the change would steepen the slope of the spectrum.

To study the possible effects of temperature differences, we use *MSX* mid-infrared and/or ATCA centimeter-continuum observations to determine the presence of embedded heating sources which are likely to be responsible for temperature differences between clumps. Figures 6 and 7 show, respectively, images of the *MSX* and ATCA emission overlayed with contours of the SIMBA 1.2 mm continuum emission. We identified by visual inspection clumps associated with extended or pointlike infrared counterparts (Fig. 6) or clumps associated with significant radio continuum (free-free) emission (Fig. 7). These clumps are likely to have embedded sources, and are indicated with black and gray contours in Figs. 6 and 7, respectively. Clumps in white and black contours (Figs. 6 and 7, respectively) appear to be free of embedded infrared or radio sources.

For the purposes of constructing the CMF, the power-law index does not depend on the temperature chosen for the whole ensemble of clumps, and the choice of higher temperatures only displaces the histogram to the left. Any slight variation of x is due to the intrinsic problem of binning the data. Nevertheless, the choice of two different temperature can change the shape of the histogram, but this change depends essentially on the ratio between the temperatures chosen rather than the values themselves.

We identified 16 out of 181 cores that appear to be warmer than the rest. For these clumps we adopt a temperature of 34 K, the average temperature of massive clumps with embedded *IRAS* sources as determined by Faúndez et al. (2004). In particular, the temperatures assigned to the cores associated with NGC 6334 I and NGC 6334 I(N), of 34 and 17 K, respectively, are in accordance with the values given by Gezari (1982). However, Sandell (2000) argues that source I is much hotter ($T_d \approx 100$ K), while

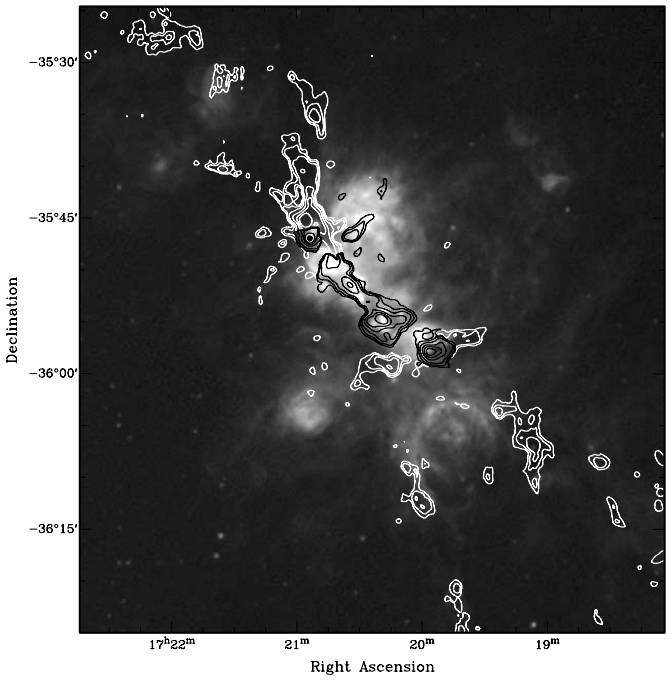

FIG. 6.—Three-color image of the *MSX* emission toward NGC 6334 (*blue*: band A, 8.28 μm; *green*: band C, 12.13 μm; *red*: band E, 21.3 μm). The contours represent the SIMBA 1.2 mm emission. Black contours indicate clumps that are associated with extended or pointlike infrared counterparts. White contours indicate the colder clumps with no infrared counterparts. [*See the electronic edition of the Journal for a color version of this figure.*]

his estimate for I(N) is 30 K, just a factor of 2 larger than our estimate. His estimate of the mass of NGC 6334 I of 200 $M_\odot$—in contrast to the 1800 $M_\odot$ in the present work—is not to be explained solely by the temperature difference, but also by the integrated flux. With a resolution of 6″ at 800 μm, his estimate

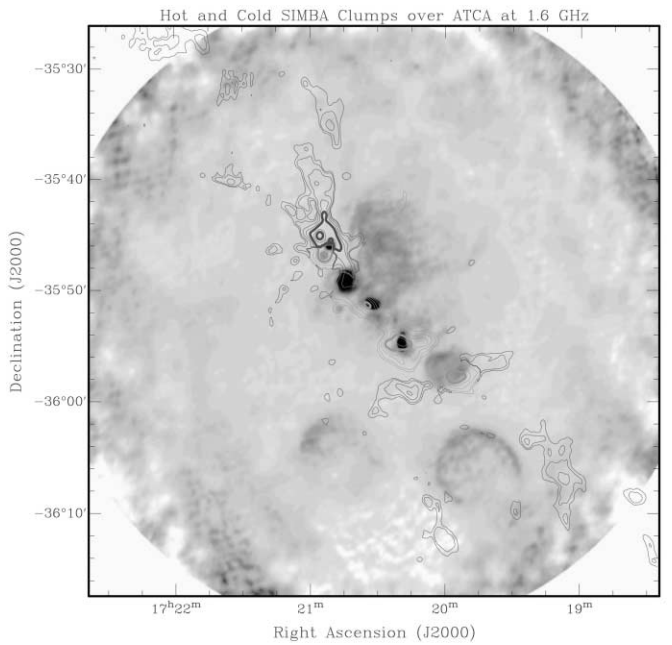

FIG. 7.—ATCA radio continuum emission at 1.6 GHz overlayed with contours of the 1.2 mm emission. Black contours indicate cold clumps having no embedded *MSX* sources and the gray contours indicate warm clumps with embedded *MSX* sources. [*See the electronic edition of the Journal for a color version of this figure.*]

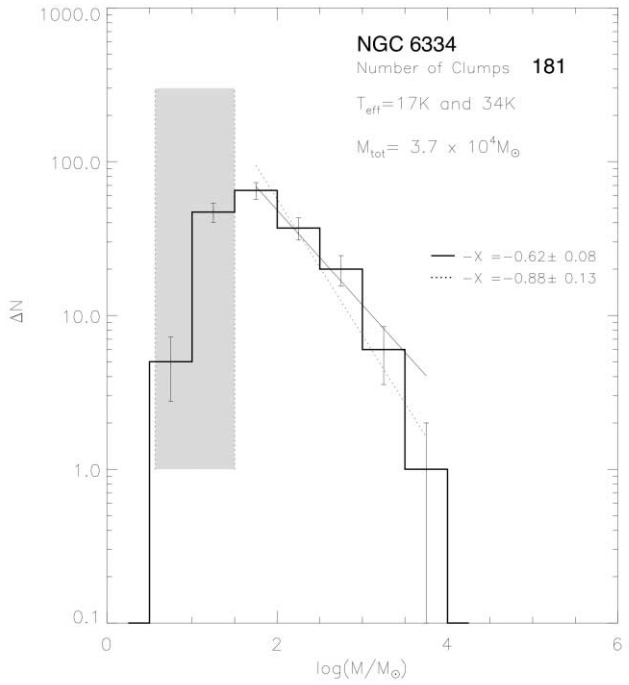

FIG. 8.—Histogram of mass distribution in NGC 6334 for a two-temperature clump ensemble: 17 and 34 K.

for the size of source I is $10'' \times 8''$, implying an effective radius ~8 times smaller than our estimate. Similarly, the definition of Sandell (2000) of NGC 6334 I(N) corresponds to the central peak of the larger clump detected by Gezari (1982). Sandell (2000) obtains a mass of 400 $M_\odot$ for source I(N), assuming a temperature of 30 K (see Sandell 2000 and references therein). Adding up the contributions from the different cores resolved within I(N) and including the surrounding cloud, Sandell (2000) finds that the mass of the whole I(N) region is ~2700 $M_\odot$. This value is in agreement with other results found in the literature and is consistent with our result after taking into account that our choice for the temperature is 17 K. We remark that estimating an exact value of the temperature for each of the clumps of the cloud is not relevant for the statistical analysis we carry out in the present work.

The newly adopted temperatures imply a repositioning of ~10% of the clumps in the mass histogram. The new mass histogram, made assuming a two-temperature cloud ensemble, is shown in Figure 8. A linear regression yields a best-fit value of $x = 0.88 \pm 0.13$ (*dotted line*), but a χ^2 fit with Poissonian error bars yields $x = 0.62 \pm 0.08$ (*solid line*). Thus, even though the warmer clumps are also preferentially the most massive, they do not concentrate solely on the most massive bin and do not affect the derived slope of the mass spectrum significantly.

The repositioning of clumps in the histogram could have a more dramatic effect when the number of clumps is considerably smaller. For example, the area NGC 6334a includes 14 of the 16 warmer clumps in NGC 6334 and a total of only 40 clumps (Fig. 5). When using two temperatures in NGC 6334a, the shape of the histogram indeed steepens, but the large relative errors yield a slope $x = 0.35 \pm 0.21$. Excluding the last bin, containing only one object, we obtain a slope of $x = 0.09 \pm 0.15$. In both cases the slope remains consistent with the value $x \sim 0.1$ from a single-temperature clump mass distribution.

TABLE 2
GAUNT FACTORS FOR FREE-FREE EMISSION

Frequency	$T = 7000$ K	$T = 8000$ K	$T = 9000$ K	$T = 10{,}000$ K
1.6 GHz.....	5.40327	5.5134	5.61051	5.69735
250 GHz.....	2.79429	2.8871	2.9702	3.04545

3.5.2. *Radio Emission Contribution*

Free-free emission is the main continuum contributor at radio frequencies. At frequencies of hundreds of gigahertz, the contribution from bremsstrahlung emission is usually neglected and all the detected emission is assumed to be due to dust. Since massive stars are being formed within NGC 6334, it is plausible that the 1.2 mm emission is not completely due to cool dust emission and that the ionized gas excited by these stars contributes an important amount. Brooks et al. (2005) studied the Keyhole Nebula and found that the 1.2 mm emission toward the H II region Car-II is strongly correlated with the 4.8 GHz continuum emission and that there is a lack of molecular line emission. They concluded that the 1.2 mm flux from the components of Car-II arise from free-free emission associated with ionized gas and not from cool dust emission associated with molecular gas.

Here we make a correction to the observed emission at 250 GHz by free-free contamination by estimating the expected ionized gas flux density at 250 GHz from the observed flux density at 1.6 GHz. Assuming that the free-free emission is optically thin at both frequencies, the ratio of the emissivities is proportional to the ratio of the $e^{-h\nu/kT_e} g_{\rm ff}(\nu, T_e)$ factors (Rybicki & Lightman 1979), where $g_{\rm ff}$ is the Gaunt factor. The exponential is essentially 1 at both frequencies. We did not use the usual radio approximation for the Gaunt factors given by Altenhoff et al. (1961), but computed them more precisely using quantum mechanical calculations, following the work of Menzel & Pekeris (Menzel & Pekeris 1935; Sommerfeld 1953). Table 2 lists the calculated Gaunt factors averaged over a Maxwell-Boltzmann distribution of velocities with temperatures between 7×10^3 and 10^4 K, typical for H II regions in massive star-forming regions (Beckert et al. 2000). At 1.6 GHz the computed Gaunt factors are only $\approx$0.3% lower than the usual Altenhoff et al. approximation. On the other hand, the calculated Gaunt factors at 250 GHz are typically 15% smaller than the values obtained from the Altenhoff et al. approximation. On the other hand, the calculated Gaunt factors at 250 GHz are typically 15% smaller than the values obtained from the Altenhoff et al. approximation (Muñoz 2006).

Table 3 summarizes the values of the estimated free-free emission at 250 GHz from selected clumps associated with H II regions (see Fig. 2). We subtracted this flux from the measured 1.2 mm flux density to estimate the actual contribution from dust, rederiving the mass of each clump. The high-mass bins are the most affected, but the best-fit exponent ($x = 0.88 \pm 0.13$) is consistent with the previous value.

3.5.3. *Binning*

Given a distribution of clump masses, the binning process invariably loses information (Rosolowsky 2005). The mass histogram can be interpreted as the derivative of a cumulative number function $\mathcal{N}(M)$, which counts clumps with mass greater than M:

$$\mathcal{N}(M) = \frac{\int_M^\infty \xi_\alpha(m)\, dm}{\int_0^\infty \xi_\alpha(m)\, dm}. \quad (5)$$

Some authors argue in favor of using the cumulative number function $\mathcal{N}(M)$ (Johnstone et al. 2000, 2001; Kerton et al. 2001; Tothill et al. 2002) to avoid the loss of information. If the cumulative number function has a power-law dependence with mass, $\mathcal{N}(M) \propto M^{-\gamma}$, then the CMF is also a power law $\xi_\alpha(M) \propto M^{-\gamma-1}$. From the definitions in § 3.4, it is clear that $\gamma = x$.

However, if there is an upper mass limit in the distribution of cores, then the cumulative mass function is not a power law, showing considerable curvature at the high-mass end. $\mathcal{N}(M)$ can be approximated by a power law with index $x = \alpha - 1$ only at masses $M \ll M_{\rm max}$ (or when $M_{\rm max} \to \infty$). For a finite upper mass limit,

$$\mathcal{N}(M) = C_1 M^{-x} + C_2, \quad (6)$$

where C_2 becomes unimportant for small masses (see Rosolowsky 2005; Reid & Wilson 2006b; Li et al. 2006). A power-law form, $\mathcal{N}(M) \propto M^{-x}$, approximates the true CMF asymptotically toward low masses. Thus, a power-law fit to the CMF must be applied within a range of masses that avoids *both* the incomplete low-mass range *and* the cutoff high-mass range. When fitting a power-law function to an observed cumulative mass function in a mass range $M > M_{\rm max}/2$ the slope invariably increases, explaining the apparent Salpeter-like slopes found in previous studies. Furthermore, the slope thus obtained is strongly dependent on the break point chosen to fit the high-mass end of the cumulative mass function and does not reflect the underlying differential clump mass distribution (ξ_α or ξ_x).

For sample sizes of $\sim$70 clumps or fewer, binning becomes an important factor in fitting a power law to differential mass functions, and the use of a cumulative mass function is preferred. Johnstone et al. (2000, 2001, 2006) and Reid & Wilson (2005, 2006a) use cumulative mass distribution functions to avoid this problem. Our sample (181 clumps) is large enough to analyze the data using either the cumulative or the differential mass functions. Figure 9 plots the normalized cumulative number function of clumps in NGC6334. A single power-law fit, which we have shown does not represent the true underlying clump mass function, gives $\mathcal{N}(M) \propto M^{-0.87}$. The dashed line in Figure 9 shows that the slope $x = 0.62$ derived from the histogram (Fig. 4) represents a good asymptote to the CMF, as predicted by the theory (eq [6]). We also show in Figure 9 a fit to the top 10% of the cloud mass [$\log(M/M_\odot) > 2.8$, *indicated by an arrow*], which yields a slope $x = 1.19$ (*dotted line*), much closer to Salpeter's value. The

TABLE 3
RADIO AN MM FLUXES (Jy) FOR SELECTED CLUMPS IN FIGURE 7

Frequency	cl1	cl19	cl169	cl11	cl27	cl7	cl210	cl4
ATCA at 1.6 GHz (free-free).....	0.59	22.77	0.45	9.42	5.28	12.61	3.49	2.89
Expected free-free at 250 GHz.....	0.31	12.16	0.24	5.03	2.82	6.73	1.86	1.54
SIMBA at 250 GHz.....	68.38	26.78	1.13	27.12	13.69	26.72	1.34	59.31

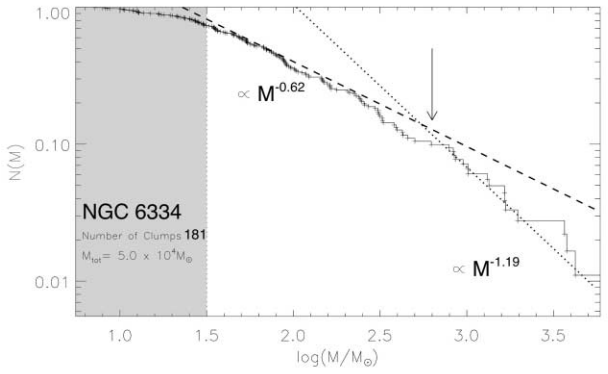

FIG. 9.—Normalized cumulative mass function $\mathcal{N}(M)$. The gray area corresponds to the region affected by completeness uncertainties as shown in Fig. 4. The arrow delimits the top 10% of the CMF, where a power-law fit to the CMF (*dotted line*) yields an apparent Salpeter-like slope.

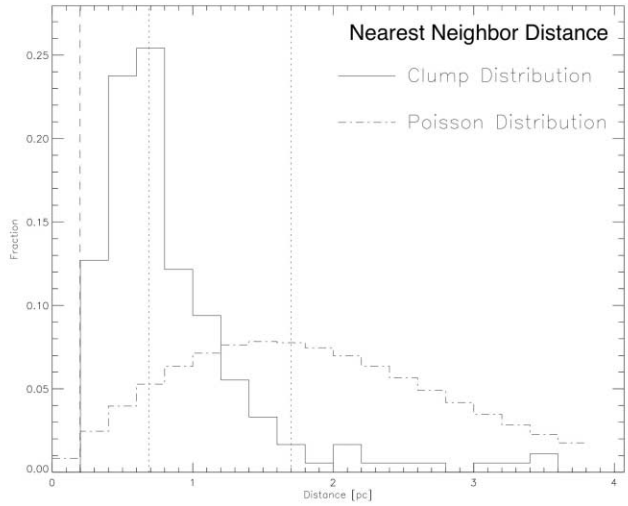

FIG. 10.—Normalized nearest neighbor distribution after dividing by 181, the number of neighbor pairs (*solid line*) and the expected distribution for random (Poisson) distribution of the same number of objects as the original sample over an identical area (*dot-dashed line*). The medians of the distributions are indicated by dotted lines.

best-fit exponent changes to $x = 1.37$ for $\log M \geq 2.9$ and to $x = 1.47$ for $\log M \geq 3.0$. Even though these slopes are consistent with Salpeter's IMF, they are an artifact of having an upper clump mass limit in the sample and do not reflect the true clump mass function

In summary, one must be aware of introducing biases when using the high-mass range to fit power laws or when fitting broken power laws to the cumulative mass function. These problems are minimized (but still present) with samples larger than 100 clumps.

3.6. *Spatial Distribution of Clumps*

In order to understand the process of fragmentation, we need to explain how masses are distributed in clumps and how they are positioned in space. A complete theory of star formation must not only reproduce the mass function, but it must explain it in all its physical implications, including how clumps, cores, and stars are distributed spatially during the evolution of the GMC (Bonnell et al. 2007). The exhaustive study of the spatial distribution of young stars in the Taurus region by Gómez et al. (1993) was extended by other authors and compiled by Larson (1995). Here we undertake a study of the degree of clustering of clumps in NGC 6334 using a similar approach.

3.6.1. *Clustering and Segregation of Clumps*

The number density of clumps can give us insight about the actual state of fragmentation and how the clumps are distributed spatially, independent of their mass. We study the number density of clumps by means of the simple grid[2] and the kernel methods.[3] Both methods require a free parameter that determines the "resolution" of the number density estimator: the binning length D in the grid technique and the smoothing length h in the kernel method, where a kernel K is defined at each pixel of the map in Figure 1 by

$$K(x,\ x_i,\ y,\ y_i) = \frac{1}{2\pi} e^{-(x^2+y^2)/2h^2}, \tag{7}$$

[2] The grid method consists in binning the two-dimensional space with squares of side l and then dividing the numbers of sources lying within each square by the area of it l^2 to obtain number density in units of length^{-2}.

[3] The kernel method (Silverman 1986) uses a kernel function K, offering the advantage that the density distribution is smoothed. In each point $(x,\ y)$ of $(\alpha,\ \delta)$, the kernel density estimator determines the density due to the contributions of all n data points.

with the kernel density estimator D defined by

$$D(x,\ y) = \frac{1}{h^2} \sum_{i=1}^{n} K(x,\ x_i,\ y,\ y_i), \tag{8}$$

where x and y are measured in parsecs, ignoring the sky curvature. The grid bin l was taken to be 2 pc, while h was chosen in order to smooth the distribution over an area πh^2, similar in size to the area over which the simple grid technique smoothed the data points (l^2).

We applied this analysis to the subregion NGC 6334b, which covers and area of $\sim$330 pc^{-2}. We find that the probability that the clumps are distributed at random within this subregion is $\sim 10^{-5}$, which argues in favor of clustered fragmentation at scales between 0.1 and 10 pc. Thus, we conclude that there is spatial segregation in clump number in addition to clump mass.

3.6.2. *The Nearest Neighbor Distribution in NGC 6334*

We calculate the nearest neighbor distribution (i.e., the frequency distribution of the linear distance to the nearest neighbor of each clump) for the clumps in NGC 6334. We neglect those clumps located too close to the edge of the mapping area but do not exclude them from the total sample, since they can be the nearest neighbor for an inner clump. We binned the nearest neighbor distances in intervals of 0.2 pc to construct the histograms shown in Figure 10. The nearest neighbor distribution is strongly skewed to small separations and is very different from the distribution expected from random positions at the same mean density. The differential probability of observing at least one event in the interval $[r_1,\ r_2]$, which defines a ring surrounding a central source, is (Gómez et al. 1993)

$$\Delta P(r_1,\ r_2,\ \eta) = e^{-\pi\eta r_1^2} - e^{-\pi\eta r_2^2}, \tag{9}$$

where $\eta = N/A$ is the average density, in this case given by $\eta = 0.11$ clumps pc^{-2}. Figure 10 compares the Poisson distribution histogram (*dashed line*) with the normalized nearest neighbor distribution for clumps. The median for the random distribution (1.7 pc) is a factor of $\sim$2.5 greater than that derived from the actual clump distribution (Fig. 10, *dotted vertical lines*).

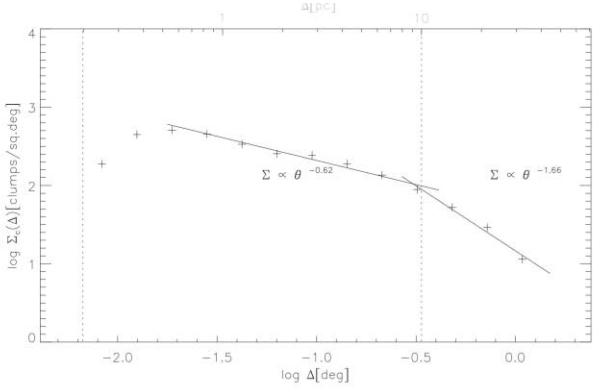

FIG. 11.—Average surface density as a function of separation in degrees (eq. [10]). The vertical dotted lines encompass the limits of validity for the fit: the beam size $\log\theta = -2.7$ ($\sim$0.2 pc) and the sampling bias (the width of subregion NGC 6334b) at $\log\theta = -0.5$, or 10 pc.

We would need to increase the average density η by a factor of 5 to produce a random distribution with the same median separation as the actual clump distribution. Thus, we conclude that the median separation of the clump distribution is significantly smaller than the expected median separation of a random distribution.

3.7. *The Average Angular Surface Density of Clumps in NGC 6334*

Most of the newly formed stars in nearby regions of star formation are located in groups or clusters. The degree of clustering of pre-main-sequence stars can be obtained by measuring their surface density as a function of angular distance, $\Sigma(\theta)$, from each star. This surface density can be fit by power laws. Gómez et al. (1993) and Larson (1995) found that there is a characteristic spatial scale ($\sim$0.04 pc) at which the surface density changes slope. This scale could mark a transition between the regime of cores within molecular clouds and protostars within cores.

We applied the approach followed by Larson (1995) to the clumps in NGC 6334, which have typical sizes $\sim$0.1 pc and separations of $\sim$1 pc. We compute $\Sigma(\theta)$ by taking each clump k and dividing the surrounding area of the sky into a set of annuli of radius θ_i (with $\theta_i = 1.5\theta_{i-1}$) and counting the number of companion clumps $\mathcal{N}_k(\theta_i)$ in each annulus (Kitsionas et al. 1998). Then

$$\Sigma(\overline{\theta_i}) = \frac{1}{N}\frac{\sum_{k=1}^{N}\mathcal{N}_k(\theta_i)}{\pi(\theta_i^2 - \theta_{i-1}^2)}, \qquad (10)$$

where $\overline{\theta_i} = (\theta_i + \theta_{i-1})/2$.

The results are plotted in Figure 11. The surface density is poorly fitted by a single power law, but the fit is much improved by using a broken power law. However, this reflects a sampling problem at large separations, since the area observed around NGC 6334 is not square. Its narrowest part has a width of $\sim$10 pc, just where the power law apparently breaks. The reliable portion of the power law has a slope of -0.62

$$\Sigma_c \propto \theta^{-0.62}, \quad 0.6 \text{ pc} \leq \theta D \leq 10 \text{ pc}, \qquad (11)$$

which is remarkably similar to the one found by Larson (1995) for separations larger than 0.04 pc calculated from young stars in the Taurus-Auriga region:

$$\Sigma_c \propto \theta^{-0.62}, \quad 0.04 \text{ pc} \leq \theta D \leq 2.5 \text{ pc}. \qquad (12)$$

These two results cover two different separation ranges in regions with widely different physical properties, yet the surface density distribution is the same. If clustering above the characteristic length of 0.04 pc maintains a self-similar behavior up to 10 pc, then the grouping of stars at large separations (between subclusters for example) could be determined from early stages of cloud fragmentation—before stars are formed.

4. DISCUSSION

The CMF and its relation to the IMF.—The clump mass function is, on the one hand, tied to the formation and evolution of *parent* molecular clouds and, on the other, to the formation of their *daughter* stars. Provided that the mechanism of clump fragmentation and collapse to form stars is universal, then the IMF should be a direct consequence of the CMF. However, since a single clump generally forms multiple stars, we cannot expect the distribution of clump masses and stellar masses to have identical functional form.

We find that the mass spectrum of clumps in NGC 6334 has a power-law dependence with mass with an index $x = 0.62$ ($dN/d\log M \propto M^{-0.62}$). This value is similar to values derived from dust continuum observations for other massive star-forming regions (Kerton et al. 2001; Tothill et al. 2002; Mookerjea et al. 2004). It is also similar to values derived from molecular line observations, usually isotopomeric lines of CO, for clouds with similar total mass. For instance, Nozawa et al. (1991) finds $\alpha = 1.7$ in Ophiuchus North (mass range of 4–250 $M_\odot$). Stutzki & Güsten (1990) finds the same exponent in M17SW (mass range of 10–3200 $M_\odot$), and Kramer et al. (1998) reports $\alpha = 1.8$ for NGC 7538 (mass range of 50–3.9×10^3 $M_\odot$). These results indicate that the clumps in all these massive star-forming regions are not the direct progenitors of individual stars. The fact that the massive clumps follow a power-law mass function over a wide range in mass is remarkable. The similarity of the "high-mass" CMF slope to the mass function of GMCs in our Galaxy (Sanders et al. 1985; Solomon et al. 1987; Pudritz 2002) seems to support a hierarchical or fractal model of the distribution of gas in the Milky Way, where fragmentation and mass distribution can be interpreted as scale free.

In order to build a complete theory of star formation we must understand the process of clustered star formation in clumps satisfying the observed CMF ($dN/d\log M \propto M^{-0.6}$) and leading to the observed IMF ($dN/d\log M \propto M^{-1.35}$). This has stimulated studies about the process of fragmentation of GMCs and clumps both theoretically and observationally. Hydrodynamic and magnetohydrodynamic numerical calculations suggest that turbulence might play a major role in the clump fragmentation process. For example, Bonnell & Davies (1998) suggest that stars are formed through the competitive accretion of gas onto protocores within molecular clouds.

Recent submillimeter and millimeter continuum observations of low-mass star-forming regions (e.g., Ophiuchus, Serpens, Orion B; Motte et al. 1998; Testi & Sargent 1998; Johnstone et al. 2000, 2001; Beuther & Schilke 2004) have revealed a CMF with a slope similar to that of the IMF. The different values obtained from the molecular line observations described above and these continuum observations probably reflects the different mass ranges sampled. In fact, dust continuum emission observations toward more distant massive star-forming regions have revealed CMF slopes consistent with a value of -0.6 (Kerton et al. 2001; Tothill et al. 2002; Mookerjea et al. 2004; this work), similar to that obtained from molecular line observations. From observations of a sample of massive clumps toward the massive star-forming region NGC 7538, Reid & Wilson (2005) concluded that a

Salpeter-like mass function is already established at the earliest stages of star formation. This is a surprising result, since many of their clumps, those with masses of 10^2–10^3 $M_\odot$, are still likely to be undergoing the process of fragmentation and cannot be direct progenitors of individual stars. Even if the structure in ISM were fractal, self-similarity would have to break on small scales, where star formation is taking place. We note, however, that the result of Reid & Wilson (2005) comes from a fit to the high-mass end of the cumulative mass function. We showed in § 3.5.3 that such fits are biased toward larger exponents. In addition to molecular line and dust continuum surveys, extinction maps can be used to map the dense molecular cores in star-forming regions. Using this technique, Alves et al. (2007) have found a mass spectrum for cores in the Pipe Nebula that is surprisingly similar to the IMF. Their CMF displaced to higher masses with respect to the stellar IMF only by a factor of 3, suggesting a one-to-one mapping from cores to stars with a star formation efficiency of ~30%. In their case the cores detected span a range of masses of approximately 1–10 $M_\odot$. This clearly indicates a much smaller scale than the clumps in our work, whether determined by the tracer or just the spatial resolution of the observations. It is not clear if the scale of the observations determines the observed fragmentation conditions—i.e., the distribution of masses—or if the IMF is a result of the complex evolution of the accreting cores and their interplay with the harboring molecular cloud and other companions. The low rate of star formation in the Pipe Nebula has led Alves et al. (2007) to suggest that this CMF can be determined at early evolutionary stages.

Assuming that at scales of 0.4 pc and masses from 100 to 5000 $M_\odot$ the *Blitz* slope ($\equiv 0.6$) is valid, the question arises: what must happen to change the slope from Blitz-like to Salpeter-like? In the context of opacity-limited gravitational fragmentation, gravitational collapse starts from density inhomogeneities and proceeds with cooling, which in turn produces smaller Jeans masses in the colder regions, favoring gravitational fragmentation on small scales. In a strictly self-similar regime, fragmentation should occur in a way that maintains the same slope in the mass spectrum at any scale. But at some point the gas cores will not be supported by thermal or nonthermal motions, collapse will occur, and stars will form, halting clump fragmentation, while larger and less dense clumps will continue fragmenting. Eventually large clump masses will be depleted, and the number of small mass clumps will increase, steepening the slope to eventually reach a Salpeter value. The exact form in which this happens is probably a combination of many of the mechanisms proposed.

Will these clumps form stars?—The discussion above assumes that all clumps fragment to form stars in order to obtain the IMF from a CMF. However, this might not be the case, in particular for some of the least massive clumps farther away from the cloud center. Are these clumps gravitationally bound? Are they hence likely to collapse? Or are they only transient structures or overdensities triggered by turbulent compressive shocks? These questions have yet to be answered, either observationally or theoretically.

Numerical simulations commonly report that many of the lower mass cores formed are not gravitationally bound (Klessen 2001; Clark & Bonnell 2005; Tilley & Pudritz 2005). Furthermore, the mass spectra can be understood as due to purely hydrodynamical effects without gravity (e.g., Clark & Bonnell 2006). As Padoan & Nordlund (2002) remark, the mass spectra resulting from turbulent fragmentation are different from the ones constructed from collapsing or unstable cores only. Only the latter form stars. These calculations show that many of the clumps could be transient structures; indeed a significant fraction of the cores end up reexpanding rather than collapsing (Vázquez-Semadeni et al. 2005; Nakamura & Li 2005), which implies that fragmentation is not sufficient to trigger star formation. If supersonic turbulence generates the initial density enhancements from which cores develop, then these cores might not necessarily approach hydrostatic equilibrium at any point in their evolution (Ballesteros-Paredes et al. 1999).

Can we distinguish observationally between bound and transient clumps? To estimate if clumps are likely or not to collapse, we need to know more about them than their mass. A clump's column density is important as a diagnostic of whether the clump is likely to collapse (Pudritz 2002). Values higher than $N \simeq 10^{22}$ cm^{-2} are observed for cores with embedded sources. The virial parameter, $M_{\rm vir}/M$, where M is a mass derived from column density and $M_{\rm vir}$ is the virial mass derived from the cloud radius and velocity dispersion (Bertoldi & McKee 1992), is known to have values close to 1.0 in star-forming clouds (Onishi et al. 1996; Yonekura et al. 2005). However, given the observational uncertainties, it is not yet clear whether this parameter is a good diagnostic for star-forming versus transient clumps.

Preferred spatial scale.—As Larson (1995) found in Taurus, there might exist a preferred scale of star formation at which clustering changes. This length can be related to the Jeans length and the Jeans mass. The surface number density of the clumps as a function of separation can reveal a characteristic spatial scale, marking a transition between clumps and cores. At separations larger than 0.6 pc and smaller than 10 pc, we find the same slope for the power-law fit to the surface density of companions as is found for the protostars in Taurus at large separations: $\Sigma \propto \theta^{-0.62}$. This finding suggests that large separations in stellar systems are determined by the position of their progenitor clumps.

5. CONCLUSIONS

We made observations of the 1.2 mm dust emission toward the giant molecular cloud NGC 6334 using the SIMBA bolometer at SEST. The main results and conclusions presented in this paper are summarized as follows.

We find 181 clumps (see Table 4 for an overview), distributed in an area of ~2.0 deg^2 centered on the main filament, which harbors most of the star-forming activity. The clumps range in size from 0.1 to 0.9 pc, with a median of 0.35 pc. This range is similar to that found by Faúndez et al. (2004) and Plume et al. (1997) for clumps in different high-mass star-forming regions. The clump masses, assuming they are isothermal, range from 3 to 6×10^3 $M_\odot$, with a completeness limit of ~30 $M_\odot$ (assuming $T_d = 17$ K).

The clump mass function (CMF) is well fit with a power-law dependence with mass, with an index $x = 0.62 \pm 0.07$ ($dN/d\log M \propto M^{-x}$) in the mass range between 30 and 6×10^3 $M_\odot$. The slope differs from the stellar IMF slope, indicating that clumps are not direct progenitors of stars. Therefore, other processes—besides fragmentation—must be important in setting up the IMF from the CMF.

We assessed possible effects on the derived slope of the CMF due to changes on the temperature assumptions and due to the contribution of free-free emission from ionized gas to the 1.2 mm emission. Although $\lesssim$10% of the clumps are likely to be significantly warmer than 17 K and are associated with regions of ionized gas, the correction for temperature and free-free emission has little effect on the derived slope.

TABLE 4
CLUMP PROPERTIES IN NGC 6334

Clump	α (J2000.0)	δ (J2000.0)	I_{peak} (Jy beam^{-1})	S_ν (Jy)	R_{eff} (pc)	$M_{1.2mm}$[a] ($M_\odot$)	M ($M_\odot$)	n[b] (cm^{-3})	Region
cl 1[c]	17 20 53.9	−35 47 1.3	17.47	68.38	0.59	4.22×10^3	1.74×10^3	3.48×10^4	NGC 6334 (6334a) (6334b)
cl 2	17 20 55.9	−35 45 17.3	14.92	95.17	0.65	5.88×10^3	5.88×10^3	8.86×10^4	NGC 6334 (6334a) (6334b)
cl 3[c]	17 20 19.8	−35 54 45.7	8.92	61.08	0.62	3.77×10^3	1.56×10^3	2.70×10^4	NGC 6334 (6334a) (6334b)
cl 4[c]	17 19 56.7	−35 57 58.0	7.15	59.31	0.86	3.66×10^3	1.47×10^3	9.69×10^3	NGC 6334 (6334a) (6334b)
cl 6[c]	17 17 1.9	−36 20 53.9	4.13	31.86	0.92	1.97×10^3	8.12×10^2	4.37×10^3	NGC 6334 (6334c)
cl 7[c]	17 20 24.4	−35 55 1.9	3.58	26.72	0.59	1.65×10^3	5.10×10^2	1.02×10^4	NGC 6334 (6334a) (6334b)
cl 8	17 20 49.9	−35 45 9.4	2.91	16.45	0.36	1.02×10^3	1.02×10^3	9.44×10^4	NGC 6334 (6334a) (6334b)
cl 9	17 20 48.0	−35 45 57.2	2.74	21.73	0.45	1.34×10^3	1.34×10^3	6.38×10^4	NGC 6334 (6334a) (6334b)
cl 10	17 20 53.9	−35 43 25.3	2.62	13.90	0.45	8.59×10^2	8.59×10^2	4.08×10^4	NGC 6334 (6334a) (6334b)
cl 11[c]	17 20 34.2	−35 51 33.8	2.30	27.12	0.71	1.68×10^3	5.63×10^2	6.54×10^3	NGC 6334 (6334a) (6334b)
cl 14[c]	17 23 16.8	−34 48 43.6	1.98	13.54	0.68	8.36×10^2	3.45×10^2	4.55×10^3	NGC 6334 (6334c)
cl 15[c]	17 20 10.5	−35 54 54.0	1.70	21.30	0.74	1.32×10^3	5.43×10^2	5.58×10^3	NGC 6334 (6334a) (6334b)
cl 16	17 20 43.4	−35 47 49.6	1.68	16.44	0.50	1.02×10^3	1.02×10^3	3.32×10^4	NGC 6334 (6334a) (6334b)
cl 19[c]	17 20 42.7	−35 49 17.4	1.36	26.78	0.68	1.65×10^3	3.73×10^2	4.92×10^3	NGC 6334 (6334a) (6334b)
cl 20	17 20 53.9	−35 42 21.2	1.29	6.93	0.36	4.28×10^2	4.28×10^2	3.97×10^4	NGC 6334 (6334a) (6334b)

NOTE.—Table 4 is published in its entirety in the electronic edition of the *Astrophysical Journal*. A portion is shown here for guidance regarding its form and content. Units of right ascension are hours, minutes, and seconds, and units of declination are degrees, arcminutes, and arcseconds.

[a] $M_{1.2mm}$ is the computed clump mass from all the emission at 1.2 mm and assuming a temperature of 17 K, while M considers the two-temperature clump ensemble and the correction by free-free emission.

[b] The average number density was computed using R_{eff} and M and assuming spherical clumps with a mean molecular weight of $\mu = 2.3$.

[c] These clumps are considered to be significantly warmer.

We investigated possible differences in the value of x among different subregions of NGC 6334. We find that the slope is significantly shallower toward the central filament ($x \approx 0.1$), which contains the most massive clumps and represents the minimum of the gravitational potential in the GMC. As we cover more extended regions, including clumps not actively forming stars, the slope steepens ($\approx 0.5,\ 0.8$), revealing that the bulk of the clumps are located in the outer areas of the molecular cloud and that these low-mass clumps predominantly determine the shape of the mass function.

We caution about the power-law–fitting procedures to the mass function. The differential CMF is sensitive to bin size and to low-number statistics in the last bin (high-mass end), as well as to completeness limits in the low-mass end. On the other hand, fitting a power law to the high-mass end of the cumulative CMF is incorrect due to its high-mass cutoff. Both the low- and high-mass ends of the cumulative CMF must be avoided in fitting power laws.

The spatial analysis performed on the two-dimensional distribution of clumps reveals that they are not distributed randomly. They are concentrated toward the center of the filament, indicating not only a segregation in mass but also a segregation in number, which could suggest a possible coalescence of massive clumps toward the gravitational potential minimum. In addition, we study the surface density of companions as a function of separation. This is well fit by a power law with a similar exponent to the one found for protostars in Taurus at large angular separations. This suggests that the position of stars in clusters is determined in the fragmentation and star formation stage rather than after dynamical relaxation.

We thank Simón Casassus and Dieter Nurnberger for helpful comments. D. J. M., D. M., G. G., and D. R. gratefully acknowledge support from the Chilean Centro de Astrofísica FONDAP 15010003.

REFERENCES

Altenhoff, W., Mezger, P. G., Wendker, H., & Westerhout, G. 1961, Veröff. Sternw., 59, 48
Alves, J., Lombardi, M., & Lada, C. J. 2007, A&A, 462, L17
Ballesteros-Paredes, J., Vázquez-Semadeni, E., & Scalo, J. 1999, ApJ, 515, 286
Beckert, T., Duschl, W. J., & Mezger, P. G. 2000, A&A, 356, 1149
Bertoldi, F., & McKee, C. F. 1992, ApJ, 395, 140
Beuther, H., Churchwell, E. B., McKee, C. F., & Tan, J. C. 2006, in Protostars and Planets V, ed. B. Reipurth, D. Jewitt, & K. Keil (Tucson: Univ. Arizona Press), 165
Beuther, H., & Schilke, P. 2004, Science, 303, 1167
Bonnell, I. A., & Davies, M. B. 1998, MNRAS, 295, 691
Bonnell, I. A., Larson, R. B., & Zinnecker, H. 2007, in Protostars and Planets V, ed. B. Reipurth, D. Jewitt, & K. Keil (Tucson: Univ. Arizona), 149
Blitz, L. 1993, in Protostars and Planets III, ed. E. H. Levy & J. I. Lunine (Tucson: Univ. Arizona Press) 125
Brooks, K. J., Garay, G., Nielbock, M., Smith, N., & Cox, P. 2005, ApJ, 634, 436
Burton, M. G., et al. 2000, ApJ, 542, 359
Carral, P., Kurtz, S. E., Rodríguez, L. F., Menten, K., Cantó, J., & Arceo, R. 2002, AJ, 123, 2574
Chini, R., Krügel, E., & Wargau, W. 1987, A&A, 181, 378
Clark, P. C., & Bonnell, I. A. 2005, MNRAS, 361, 2
———. 2006, MNRAS, 368, 1787
Evans, N. J., II. 1999, ARA&A, 37, 311
Faúndez, S., Bronfman, L., Garay, G., Chini, R., Nyman, L.-Å., & May, J. 2004, A&A, 426, 97
Garay, G., Brooks, K. J., Mardones, D., Norris, R. P., & Burton, M. G. 2002, ApJ, 579, 678
Gezari, D. Y. 1982, ApJ, 259, L29
Gómez, M., Hartmann, S., Kenyon, S. J., & Hewett, R. 1993, AJ, 105, 1927
Hunter, T. R., Brogan, C. L., Megeath, S. T., Menten, K. M., Beuther, H., & Thorwirth, S. 2006, ApJ, 649, 888
Jackson, J. M., & Kraemer, K. E. 1999, ApJ, 512, 260
Johnstone, D., Fich, M. Mitchell, G. F., & Moriarty-Schieven, 2001, ApJ, 559, 307
Johnstone, D., Matthews, H., & Mitchell, G. F. 2006, ApJ, 639, 259
Johnstone, D., Wilson, C. D., Moriarty-Schieven, G., Joncas, G., Smith, G., Gregersen, E., & Fich, M. 2000, ApJ, 545, 327
Kerton, C. R., Martin, P. G., Johnstone, D., & Ballantyne, D. R. 2001, ApJ, 552, 601
Kitsionas, S., Gladwin, P. P., & Whitworth, A. P. 1998, in ASP Conf. Ser. 132, Star Formation with the Infrared Space Observatory, ed. J. Yun & R. Liseau (San Francisco: ASP), 434

Klessen, R. S. 2001, ApJ, 556, 837
Klessen, R. S., & Burkert, A. 2000, ApJS, 128, 287
Kraemer, K. E., & Jackson, J. M. 1999, ApJS, 124, 439
Kramer, C., Stutzki, J., Rörig, R., & Corneliussen, U. 1998, A&A, 329, 249
Kroupa, P. 2001, MNRAS, 322, 231
Lada, C. J., & Lada, E. A. 2003, ARA&A, 41, 57
Lada, E. A. 1999, in The Origin of Stars and Planetary Systems, ed. C. J. Lada & N. D. Kylafis (Dordrecht: Kluwer), 441
Larson, R. 1995, MNRAS, 272, 213
Larson, R. B. 2003, in ASP Conf. Ser. 287, Galactic Star Formation Across the Stellar Mass Spectrum, J. M. De Buizer & N. S. van der Blick (San Francisco: ASP), 65
Li, D., Velusamy, T., Goldsmith, P. F., & Langer, W. D. 2006, preprint (astro-ph/0610634)
McBreen, B., Fazio, G. G., Stier, M., & Wright, E. L. 1979, ApJ, 232, L183
McCutcheon, W. H., Sandell, G. Matthews, H. E., Kuiper, T. B. H., Sutton, E. C., Danchi, W. C., & Sato, T. 2000, MNRAS, 316, 152
Menzel, D. H., & Pekeris, C. L. 1935, MNRAS, 96, 77
Mookerjea, B., Kramer, C., Nielbock, M., & Nyman, L.-Å. 2004, A&A, 426, 119
Moran, J. M., Greene, B., Rodriguez, L. F., & Backer, D. C. 1990, ApJ, 348, 147
Motte, F., Andre, P., & Neri, R. 1998, A&A, 336, 150
Motte, F., Schilke, P., & Lis, D. C. 2003, ApJ, 582, 277
Muñoz, D. J. 2006, M.S. thesis, Univ. Chile
Nakamura, F., & Li, Z.-Y. 2005, ApJ, 631, 411
Neckel, T. 1978, A&A, 69, 51
Nozawa, S., Mizuno, A., Teshima, Y., Ogawa, H., & Fukui, Y. 1991, ApJS, 77, 647
Onishi, T., Mizuno, A., Kawamura, A., Ogawa, H., & Fukui, Y. 1996, ApJ, 465, 815
Ossenkopf, V., & Henning, T. 1994, A&A, 291, 943
Padoan, P., & Nordlund, Å 2002, ApJ, 576, 870
Plume, R., Jaffe, D. T., Evans, N. J., II, Martin-Pintado, J., & Gomez-Gonzalez, J. 1997, ApJ, 476, 730
Pudritz, R. E. 2002, Science, 295, 68
Reid, M. A., & Wilson, C. D. 2005, ApJ, 625, 891
———. 2006a, ApJ, 644, 990
———. 2006b, ApJ, 650, 970
Rodríguez, L. F., Cantó, J., & Moran, J. M. 1982, ApJ, 255, 103
Rosolowsky, E. 2005, PASP, 117, 1403
Rybicki, G. B., & Lightman, A. P. 1979, Radiative Processes in Astrophysics (New York: Wiley Interscience)
Salpeter, E. E. 1955, ApJ, 121, 161
Sandell, G. 2000, A&A, 358, 242
Sanders, D. B., Scoville, N. Z., & Solomon, P. M. 1985, ApJ, 289, 373
Scalo, J. 1998, in ASP Conf. Ser. 142, The Stellar Initial Mass Function, ed. G. Gilmore & D. Howell (San Francisco: ASP), 201
Schneider, N., & Brooks, K. 2004, Publ. Astron. Soc. Australia, 21, 290
Silverman, B. W. 1986, Monographs on Statistics and Applied Probability (London: Chapman and Hall)
Solomon, P. M., Rivolo, A. R., Barrett, J., & Yahil, A. 1987, ApJ, 319, 730
Sommerfeld, A. J. F. 1953, Atombau und Spektrallinien, Vol. 2 (New York: Unger)
Straw, S. M., & Hyland, A. R. 1989, ApJ, 340, 318
Straw, S. M., Hyland, A. R., & McGregor, P. J. 1989, ApJS, 69, 99
Stutzki, J., & Güsten, R. 1990, ApJ, 356, 513
Testi, L., & Sargent, A. I. 1998, ApJ, 508, L91
Tilley, D. A., & Pudritz, R. E. 2005, MNRAS, submitted (astro-ph/0508562)
Tothill, N. F. H., White, G. J., Matthews, H. E., McCutcheon, W. H., McCaughrean, M. J., & Kenworthy, M. A. 2002, ApJ, 580, 285
Vázquez-Semadeni, E., Kim, J., Shadmehri, M., & Ballesteros-Paredes, J. 2005, ApJ, 618, 344
Ward-Thompson, D., Andre, P., Crutcher, R., Johnstone, D., Onishi, T., & Wilson, C. 2007, in Protostars and Planets V, ed. B. Reipurth, D. Jewitt, & K. Keil (Tucson: Univ. Arizona), 33
Williams, J. P., Blitz, L., & McKee, C. F. 2000, in Protostars and Planets IV, ed. V. Mannings, A. P. Boss, & S. S. Russell (Tucson: Univ. Arizona), 97
Williams, J. P., de Geus, E. J., & Blitz, 1994, ApJ, 428, 693
Yonekura, Y., Asayama, S., Kimura, K., Ogawa, H., Kanai, Y., Yamaguchi, N., Barnes, P. J., & Fukui, Y. 2005, ApJ, 634, 476